

## RESEARCH ARTICLE OPEN ACCESS

# N-Type Behavior from a P-Type Dopant: Charge Compensation Mechanisms in Trivalent Y-Doped HfO<sub>2</sub>

Oliver Rehm<sup>1</sup>  | Lutz Baumgarten<sup>2</sup>  | Florian Wunderwald<sup>3</sup>  | Andreas Fuhrberg<sup>1</sup>  | Pia Maria Düring<sup>1</sup> | Andrei Gloskovskii<sup>4</sup> | Christoph Schlueter<sup>4</sup> | Thomas Mikolajick<sup>3,5</sup> | Uwe Schroeder<sup>3</sup> | Martina Müller<sup>1</sup>

<sup>1</sup>Fachbereich Physik, Universität Konstanz, Konstanz, Germany | <sup>2</sup>Forschungszentrum Jülich GmbH, Peter Grünberg Institut (PGI-6), Jülich, Germany | <sup>3</sup>NaMLab gGmbH, Dresden, Germany | <sup>4</sup>Deutsches Elektronen-Synchrotron, Hamburg, Germany | <sup>5</sup>Technische Universität Dresden, Dresden, Germany

**Correspondence:** Martina Müller ([martina.mueller@uni-konstanz.de](mailto:martina.mueller@uni-konstanz.de))

**Received:** 20 August 2025 | **Revised:** 1 October 2025 | **Accepted:** 8 October 2025

**Keywords:** HAXPES | HfO<sub>2</sub> | oxygen vacancies (OVs) | p-doping limit

## ABSTRACT

The current market launch of HfO<sub>2</sub>-based ferroelectric devices relies on the control of the inherent oxygen vacancies (OVs) and their impact on the ferroelectric performance. Due to the necessary stabilization of the ferroelectric phase by doping, several dopants are investigated for their applicability to control the vacancy concentration. Hf<sup>3+</sup> signatures in X-ray photoemission spectra are often used as an indication of OVs for both qualitative and quantitative analysis. The analysis of Y doped HfO<sub>2</sub> (Y:HfO<sub>2</sub>) as investigated by hard x-ray photoelectron spectroscopy (HAXPES) reveals the inapplicability of the Hf<sup>3+</sup> signature for a quantitative determination of OVs in the case of heterovalent doping and is restricted to pure HfO<sub>2</sub> or isoelectronic substitution of Hf by, for example, Zr.

## 1 | Introduction

Within the last decade, complementary metal-oxide-semiconductor (CMOS)-compatible ferroelectric materials based on HfO<sub>2</sub> and AlN have been discovered [1, 2]. This has boosted interest and investigations into ferroelectric devices such as ferroelectric random access memories (FeRAM)[3], field-effect transistors (FeFET)[4], or tunnel junctions (FTJ)[5]. In all cases the functionality of HfO<sub>2</sub>-based ferroelectric devices has already been proven. However, reliability problems like wake-up, fatigue, and imprint effects currently hamper a broad commercial market launch. The reliability issues are mainly related to oxygen vacancy (OV) defects in HfO<sub>2</sub> [6, 7]. Since the switchable ferroelectric state in these new CMOS-compatible materials has to be stabilized by doping, the choice of dopants may strongly affect the vacancy formation and concentration.

Several elements have been proven theoretically and experimentally to stabilize the ferroelectric phase in HfO<sub>2</sub> by cation

substitution (e.g., Si [8], Al [9], Zr [10], Y [11, 12], Gd [13], La [14], Sr [15], Ta [16, 17]). But even without doping, a certain amount of oxygen defects can stabilize the ferroelectric state [18, 19]. Depending on their most stable oxidation state, these elements can be grouped into an isovalent substitution of Hf in HfO<sub>2</sub> (e.g., Si<sup>4+</sup>, Zr<sup>4+</sup>) and a heterovalent doping (e.g., La<sup>3+</sup>, Y<sup>3+</sup>, Ta<sup>5+</sup>). Currently, the isovalent cation substitution of Hf by 50 % Zr (HZO) is the method of choice to stabilize the ferroelectric phase. However, the reliability problem based on OV defects remains unsolved.

Stabilizing the ferroelectric phase by heterovalent cation doping, for example, La, Y, or Ta [16, 17, 11, 14] requires an additional charge compensation, which may be either ionic or electronic [20, 11]. Considering only ionic charge compensation by OV or interstitials, an increased OV concentration for trivalent elements like Y or La and an increased oxygen interstitial concentration for pentavalent elements like Ta is expected [17, 21]. The tetravalent Hf substitution by Zr should not directly affect the vacancy concentration since no doping charge compensation is required.

This is an open access article under the terms of the [Creative Commons Attribution](https://creativecommons.org/licenses/by/4.0/) License, which permits use, distribution and reproduction in any medium, provided the original work is properly cited.

© 2025 The Author(s). *Advanced Physics Research* published by Wiley-VCH GmbH

Here changes in the defect density are induced indirectly, either by the production process or by induced lattice strain.

Due to the fact that also an isovalent substitution of Hf is possible to stabilize the ferroelectric phase and heterovalent doping is not strictly necessary, the heterovalent valency may be used as a possible parameter to adjust the defect density, which may be achieved by co-doping [22]. However, a systematic investigation of this possibility is currently lacking. Here, the in-depth investigation of trivalent Y doping of  $\text{HfO}_2$  ( $\text{Y:HfO}_2$ ) and its relation to the defect concentration is presented. We discuss in detail the possible doping charge compensation mechanisms and their consequences for the electronic and ferroelectric structure.

Hard X-ray photoelectron spectroscopy (HAXPES) is an ideal probe of these ionic and electronic changes. Collective core level rigid shifts directly represent the change in Fermi level energy and an individual core level binding energy BE shift indicates different chemical and valence states.

In all cases, the position of the Fermi level within the band gap determines the kind of charge compensation, either ionic, electronic, or both and can be taken as an indicator for the relevant charge compensation mechanism. This applies not only to the bulk but also to interface band alignments [20, 23].

Using HAXPES, we investigated the rigid BE shift of trivalent doped  $\text{Y:HfO}_2$ , which we can directly relate to the change of the Fermi level. In contrast to an expected p-doping behavior of the trivalent Y, we observed an n-doping shift of the Fermi level. We relate this to an ionic charge compensation in contrast to electronic hole doping. However, the observed Fermi level shift suggests an overcompensation of the induced Y doping charge. In addition we critically discuss the use of an  $\text{Hf}^{3+}$  signature in HAXPES spectra for a qualitative and quantitative estimate of OVs in the case of heterovalent doped  $\text{HfO}_2$ .

## 2 | Results

Figure 1 shows an HAXPES overview spectrum of a TiN (10 nm)-capped  $\text{Y:HfO}_2$  sample with an Y-doping concentration of 2.9 % (black), recorded at 6 keV photon energy and  $5^\circ$  emission angle, with an information depth of approximately 15 nm. The N 1s, Hf 4f, N 2s core levels, as well as the valence band (VB) BE regions are shown. In addition, a spectrum of a pure TiN reference sample is given (red curve). To enable a quantitative comparison, the TiN reference spectrum was rescaled to match the N 1s signal intensity of the TiN-capped  $\text{Y:HfO}_2$  sample. This normalization allows comparison of the peak shapes, intensities and BE positions of sample and reference. The visible shoulder at 396 eV within the N 1s core level peak of the TiN-capped  $\text{Y:HfO}_2$  sample is related to the formation of HfN at the TiN/ $\text{Y:HfO}_2$  interface, which is absent in the pure TiN reference sample [18].

The inset of Figure 1 shows the Hf 4f BE region between 15 eV and 20 eV

BE. This BE region is of particular importance due to possible  $\text{Hf}^{3+}$  signatures [23, 18, 24, 25]. This feature is typically related to the emergence of OVs.

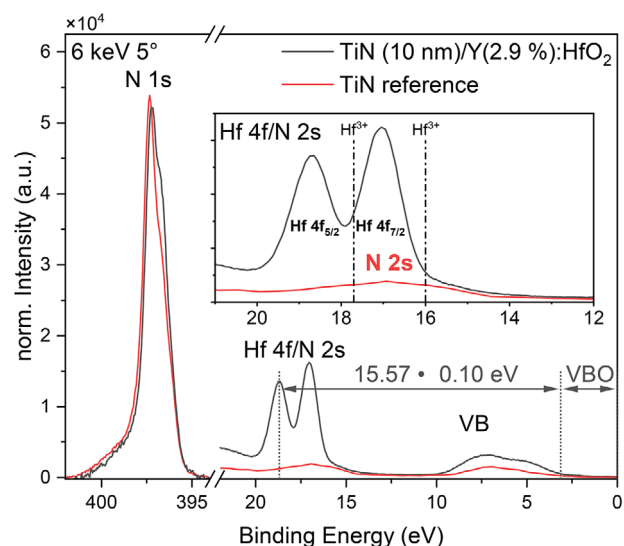


**FIGURE 1** | HAXPES spectra of N 1s, Hf 4f, N 2s core level, and valence band (VB) BE regions acquired using 6 keV photon energy at  $5^\circ$  emission angle. The black curve corresponds to the TiN (10 nm)-capped  $\text{Y(2.9 %):HfO}_2$  sample, and the red curve represents the TiN reference.

A key observation can be derived: in TiN/ $\text{HfO}_2$  bilayers, the N 2s core level peak at  $\sim 17$  eV overlaps with the low BE region of the Hf 4f  $_{7/2}$  peak that is typically identified as  $\text{Hf}^{3+}$  component at  $\sim 16.5$  eV and used for quantitative analysis. But whenever an N-component is present in a spectrum, obviously, it is particularly difficult to separate these individual elemental contributions, and extreme care should be taken when fitting peak intensities. Therefore, we avoid deconvoluting a possible  $\text{Hf}^{3+}$  component from the N 2s emission.

Alternatively, our analysis focuses on the BE position and -shift of the spin-orbit split Hf 4f  $_{5/2}$  core level peak side, as this peak should be negligibly affected by the superposition of the N 2s core level peaks compared to the Hf 4f  $_{7/2}$  core level peak. In addition, as we will discuss below, in the case of heterovalent doping the emergence of a  $\text{Hf}^{3+}$  component cannot be used as a qualitative or quantitative measure for OVs. In Figure 1, we also include the BE difference between the Hf 4f  $_{5/2}$  peak and the VB maximum (VBM). The VBM is determined by a linear fit to the slope of the VB top edge and its intersection with a constant background. Together with the rigid shift of the Hf 4f  $_{5/2}$ , the VB offset (VBO) is calculated for the samples with different Y concentrations.

Figure 2 presents the analysis of HAXPES Hf 4f core level rigid shifts of Y-doped  $\text{HfO}_2$  ( $\text{Hf}_{1-x}\text{Y}_x\text{O}_2$ ) for Y concentrations ranging from  $x = 2.9\%$  to  $x = 17.1\%$ , obtained using 6 keV photon energy. The Y-doping content was assessed through cross-section corrected intensity comparisons of the Hf 4p and Y 3p core level peaks [26, 27].

In Figure 2a the rigid shift of the Hf 4f doublet is shown and compared to an undoped  $\text{HfO}_2$  sample, which showed no indications of  $\text{Hf}^{3+}$  related to OVs. This sample was previously analyzed in detail by L. Baumgarten et al. in a study focusing on  $\text{Hf}^{3+}$  and OVs [18]. This spectrum serves as a reference for identifying rigid shifts of the other Hf 4f spectra. In comparison to this reference, the  $\text{HfO}_2$  layers doped with trivalent Y concentrations of 2.9 %, 4.4 %, and 17.1 % showed rigid shifts of the Hf 4f doublet towards lower BE values.

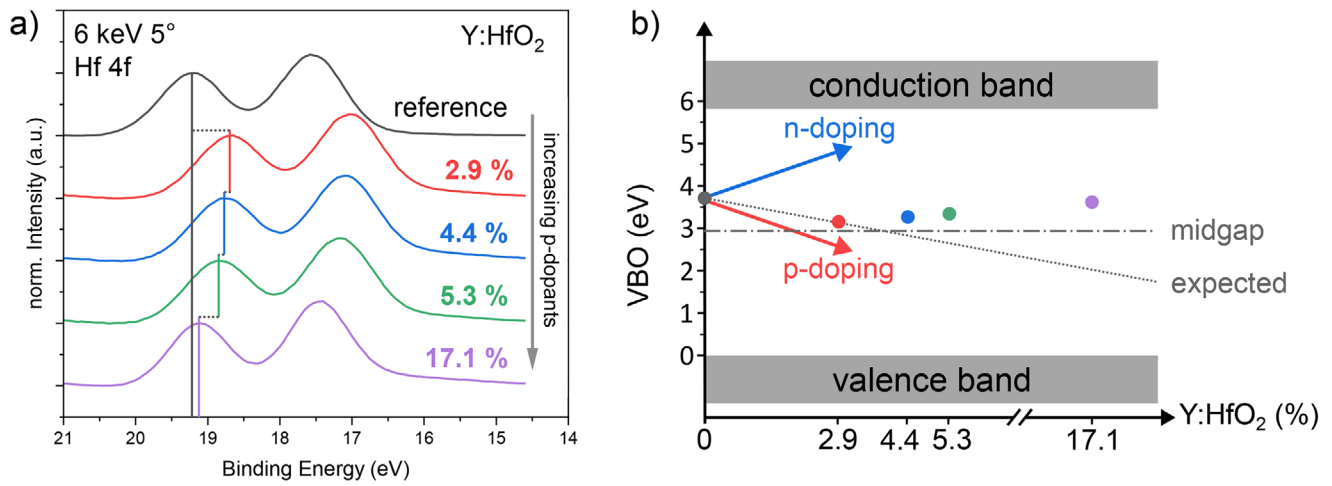


**FIGURE 2** | (a) HAXPES Hf 4f core level spectra of different Y-doped HfO<sub>2</sub> layers measured at a photon energy of 6 keV. (b) Depicts the rigid BE shift in form of VBO obtained from the Hf 4f spectra as a function of Y-doping percentage. The observed trend indicates a transition from p- to n-type doping behavior, with a p-doping limit close to midgap.

5.3 %, and 17.1 % all exhibit shifts toward lower BE, consistent with p-type doping.

Figure 2b illustrates the VBO over Y-doping content in HfO<sub>2</sub> in comparison to an expected pure n or p-doping behavior. In the case of trivalent Y one might expect the p-doping shift towards lower BE as observed for the 2.9 % Y-doping would continue similarly for the 4.4 % and higher Y concentrations. However, the observation suggests otherwise. In reality, as the Y content increases beyond the 2.9 %, the Hf 4f spectrum shifts towards higher

BE as expected for an n-doping direction. This indicates that a p-doping limit has been reached; further addition of trivalent dopants leads to a transition to n-type behavior. The importance of the doping limit in HfO<sub>2</sub> has been discussed in detail theoretically and experimentally [23, 28, 29]. We estimated the p-doping limit at a VBO of about 3 eV close to the midgap dashed-dotted line. This value is in agreement with our previous investigation of the band alignment at TiN interfaces [23] and indicates an oxygen-poor condition of the samples [28]. The doping limit is determined by the spontaneous creation possibility of OV, which depends on the defect formation energy as a function of the Fermi level position. The actual value varies with the already existing OV concentration.

All spectra have also been recorded with a photon energy of 2.8 keV. Although the information depth (ID) is reduced to about 9 nm the Hf 4f level is still visible due to the exponential decay of the ID. However, its intensity is strongly reduced. Compared to the 6 keV measurement, only minor differences are observed in shape and rigid shift, and thus, the spectra are not shown here.

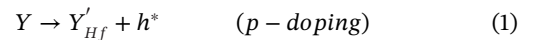
### 3 | Discussion

The rigid core level shift, as observed for different Y concentrations in Figure 2 indicates a strong doping dependence of the Fermi level on the trivalent Y ion. This rigid shift is exclusively related to a shift of the Fermi level within the band gap and is

equivalent for all core levels related to the HfO<sub>2</sub> layer. However, in contrast to the rigid shift toward lower BE, as expected for p-doping of a trivalent ion, the Hf 4f core levels exhibits a complex behavior with a shift toward lower BE at low Y concentrations, as expected, but a reversed shift, back to the undoped case with further increasing Y concentrations, as expected for n-doping. At this stage, a detailed examination of the potential charge compensation mechanisms in doped HfO<sub>2</sub> and their relationship to the Fermi level position will be conducted. In particular, it allows for an experimental distinction of different compensation mechanisms based on the Fermi level position in these different cases.

#### 3.1 | Trivalent Doping

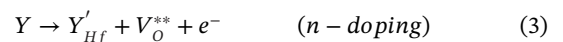
The cation doping of HfO<sub>2</sub> by a trivalent element like Y, leads to a missing electron at an oxygen site. In a purely electronic view, this creates a hole in the VB and is well known as p-doping in semiconductors like Si or GaAs. In other words, the missing valence electron is electronically compensated by a valence hole. In Kröger-Vink notation, this may be written as:



Here,  $Y'_{Hf}$  indicates a Y<sup>3+</sup> ion at a Hf<sup>4+</sup> lattice site and  $h^*$  an electronic hole in the VB. The prime indicates a negative charge compared to a 4+ Hf site. However, there are two alternative ways to compensate for the missing valence electron. Within the pure ionic path, an OV,  $V_O$  in Kröger-Vink notation, may supply two electrons, compensating the lacking electrons of two Y ions.



Within a mixed compensation, the vacancy will compensate only one Y ion, leaving one electron for n-doping.



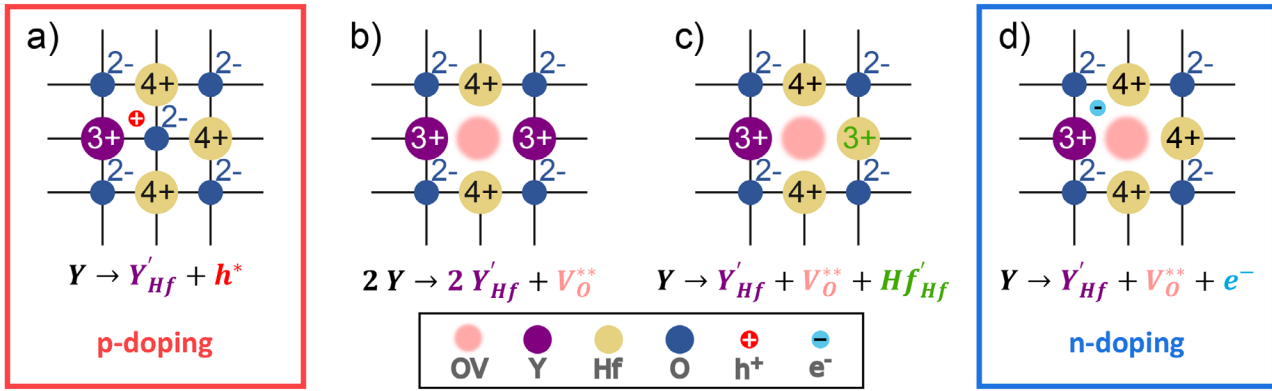
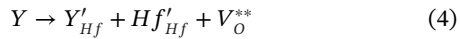


**FIGURE 3** | Graphical illustration of the four different Y-doping mechanisms in  $\text{HfO}_2$ , as discussed in Equations (1) to (4). The transition from p- to n-type doping behavior is influenced by the formation of OVs, with the independent formation of OVs from  $\text{Hf}^{3+}$  also depicted. Only mechanism (c) exhibits a direct dependence between  $\text{Hf}^{3+}$  and OVs.

Thus, depending on the charge compensation mechanism, a group III element may act as n- or p-dopant.

Experimentally, the appearance of an  $\text{Hf}^{3+}$  spectral component is often taken as a signature for OV and sometimes used for a quantification of the vacancy concentration [18, 30]. However, a  $\text{Hf}^{3+}$  component ( $\text{Hf}'_{\text{Hf}}$ ) does not appear in relation (1) to (3). A compensation process leading to  $\text{Hf}^{3+}$  component may be included as:



and is also a pure ionic path equivalent to the compensation path described in relation (2). Both ionic compensation paths (relation (2) and (4)) are schematically sketched in Figure 3b,c. It should be noted that relation (4) with the related Figure 3c is the only compensation path, which leads to an observable  $\text{Hf}^{3+}$  component within the photoemission spectra. Thus, a missing  $\text{Hf}^{3+}$  spectral signature does not indicate a negligible vacancy concentration, and an observed  $\text{Hf}^{3+}$  spectral signature cannot be taken as a quantitative measure for the vacancy concentration.

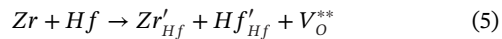
OVs, as described in relations (2)–(4), may not exclusively be created by the trivalent doping but also by lattice strain or oxygen deficiency during sample growth. Thus, relations (2)–(4) may also be taken as compensation paths for existing vacancy charges by trivalent doping. Experimentally, the different compensation paths can be distinguished by the behavior of the Fermi level. An undoped, perfect  $\text{HfO}_2$  sample should exhibit a Fermi level position close to midgap, with a VBO of about 3 eV. The electronic compensation of relation (1) should be accompanied by a Fermi level shift toward the VB, like in p-doping of conventional semiconductors like Si or GaAs [31]. The reverse applies for the mixed compensation of relation (3), which should show a Fermi level shift toward the conduction band and core level shifts toward higher BE. The pure ionic compensation paths (relations (2) and (4)) should not result in a change of the Fermi level and thus not in a rigid shift of the observed core levels, since no free carriers (electrons or holes) are created. Both pure ionic paths might be distinguished by the creation of a  $\text{Hf}^{3+}$  spectral signature. However, it should be noted, that relation (1)–(4) describe ideal charge compensation. In reality, an incomplete charge compensation, in particular in relations (2) and (4), may

experimentally lead to a small n-doping behavior of the core level shifts.

In view of the above discussion, we can relate the observed rigid shifts to the individual charge compensation paths. However, a first remark considers the reference sample. Although no  $\text{Hf}^{3+}$  signatures are observed, the sample cannot be taken as defect-free, since it was proven to be ferroelectric and without doping the ferroelectric phase has to be stabilized by defects [19]. Accordingly, the observed VBO of 3.7 eV implies a Fermi level shifted by about 0.7 eV from the equilibrium midgap position towards the conduction band (n-doping). The observed rigid shift towards lower BE for the lowest Y concentration indicates a p-doping and thus an electronic charge compensation (relation (1)). The observed VBO of 3.1 eV implies a Fermi level close to its equilibrium midgap position. Thus, the Y doping compensates n-doping effects by existing OVs. However, for all higher Y dopant concentrations we observe a rigid shift toward higher binding energies as expected for n-doping. Thus, experimentally we conclude that the mixed compensation mechanism of relation (3) is the dominant compensation path. Now the question arises, why the dominant charge compensation path changes from a p-doping to n-doping behavior?

Since doping in general shifts the position of the Fermi level, a closer look at the defect formation as a function of Fermi energy is useful.  $\text{HfO}_2$  is known to have a very limited doping range [28]. An attempt to shift the Fermi level out of this range results in the creation of defects for compensation. An attempt to shift the Fermi level toward the VB, for example, with p-doping, in general results in the creation of  $V_{\text{O}}^{**}$  defects since these are energetically the most favorable defects. However, with the creation of  $V_{\text{O}}^{**}$  defects, the compensation path of Equation (1) is obsolete. Nevertheless, for a low doping concentration, keeping the Fermi level within the “allowed” doping range, a p-doping behavior is possible. This behavior is observed as a rigid shift towards lower binding energies between an undoped sample and one doped with 2.9 % Y-doped sample as shown in Figure 2. The pure ionic path of Equation (2) is considered unlikely, since it requires two doping atoms in the vicinity of the OV. At low doping ranges, this possibility may be neglected. The ionic path as described by Equation (4) with the creation of a  $\text{Hf}^{3+}$  ion might be possible. However, a Fermi level shift is not expected in this case.

Finally, we may add some remarks on the difference between heterovalent doping and isovalent cation substitution. In case of isoelectronic substitution of Hf by, for example, Si or Zr no doping charge has to be compensated. Nevertheless, vacancies are usually created due to lattice strain caused by the different ionic radii or due to an oxygen deficiency in the preparation process. In this case, not the doping charge but the vacancy charge has to be compensated. In terms of Kröger-Vink notation for HZO, this may be written as:



Equivalently, two  $\text{Hf}^{3+}$  ions will compensate a single  $V_{\text{O}}^{**}$  in pure  $\text{HfO}_2$ . An incomplete compensation of these vacancy charges by  $\text{Hf}^{3+}$  or  $\text{Zr}^{3+}$  leads to an n-doping behavior [18]. Whereas in heterovalent doping a relation between an  $\text{Hf}^{3+}$  spectral intensity and the OV density is not possible in isovalent substitution this relation can be drawn in assuming a complete charge compensation by  $\text{Hf}^{3+}$  and/or  $\text{Zr}^{3+}$ .

Thus, in general, the appearance of an  $\text{Hf}^{3+}$  spectral component indicates the existence of an OV but its absence cannot be taken as an indication of a negligible OV concentration. A direct relation between  $\text{Hf}^{3+}$  and OVs seems to be possible only for pure, undoped  $\text{HfO}_2$ .

## 4 | Conclusion

Contrary to the expected p-type doping behavior associated with trivalent doping by Y, a general n-type doping behavior of the Fermi level is observed. Only the lowest investigated Y concentration exhibits the expected p-doping behavior. An analysis of the possible charge compensation mechanisms in oxide insulators in combination with the limited doping range of  $\text{HfO}_2$  leads to a consistent explanation of the complex behavior of the Fermi level. Here, the single Y doping charge is compensated by an OV charge, with the second electron of the vacancy leading to the observed n-type doping behavior. The analysis of the possible charge compensation paths reveals some additional information regarding the quantification of OVs. In general, the  $\text{Hf}^{3+}$  signature in PE spectra cannot be used as a quantitative measure of OVs. In the case of heterovalent doping, the appearance of  $\text{Hf}^{3+}$  is related only to one of at least four possible charge compensation paths. Only in pure  $\text{HfO}_2$  and in an isovalent cation substitution, e.g., by Zr (HZO), this quantification is possible. However, in the case of HZO, both the creation of  $\text{Hf}^{3+}$  and  $\text{Zr}^{3+}$  have to be taken into account. Due to the necessity of OVs for charge compensation, the trivalent, doping may be used to compensate the charge of residual vacancies, as created by lattice strain or oxygen deficiency in the sample growth, as long as the Fermi level keeps inside the allowed doping range. Otherwise, the trivalent Y doping leads to the creation of additional vacancies for the compensation of doping charges.

## 5 | Experimental Section

The samples were deposited on p-Si substrates. First, a 30 nm tungsten (W) layer was deposited using physical vapor deposition (PVD), followed by a 10 nm titanium nitride (TiN) layer, also

deposited via PVD. Subsequently, a 10 nm-thick Y-doped  $\text{HfO}_2$  ( $\text{Y:HfO}_2$ ) layer was deposited using atomic layer deposition (ALD). The Y concentration in the  $\text{HfO}_2$  films was varied (2.9 %, 4.4 %, 5.3 %, and 17.1 %) by switching the Hf precursor from tris(dimethylamido)cyclopentadienyl hafnium  $\text{Hf}(\text{C}_5\text{H}_5)(\text{N}(\text{CH}_3)_2)_3$  to the Y precursor (ARYA, Air Liquide). Ozone was used as the reactant for  $\text{HfO}_2$  deposition, while oxygen plasma was used as the reactant for  $\text{YO}_2$ . To prevent air exposure and prepare the sample for device integration, a capping layer of 10 nm TiN was deposited using PVD. Finally, the entire stack underwent thermal annealing at 500 ° C for 20 s.

The stoichiometry of the  $\text{Y:HfO}_2$  layer was determined using HAXPES at a photon energy of 6 keV and an emission angle of 5 °. The Y:Hf ratio was calculated based on the intensities of the Y 3p, Y 3d, Hf 4p, and Hf 4d peaks, weighted by their respective photoionization cross sections [26, 27].

HAXPES was performed at the P22 beamline of PETRA III (DESY, Hamburg)[32] to investigate element-selective chemical properties. Core level spectra of Hf 4f, O 1s, Y 3p, Ti 2p, and N 1s, were recorded at photon energies of 2.8 and 6 keV, providing information depths of 9 and 15 nm, respectively. These depths correspond to approximately 95 % of the signal. The information depths were estimated using the Electron Spectra for Surface Analysis (SESSA) from the National Institute of Standards and Technology (NIST) [33]. A SPECS PHOIBOS 225HV electron analyzer was used at an emission angle of 5 ° and a pass energy of 50 eV, resulting in an overall energy resolution of approximately 300 meV.

### Acknowledgments

This work received funding from the BMBF (project 05K22VLI), by University of Konstanz BlueSky initiative and by the VECTOR Foundation (project iOSMEMO), and was supported by the Deutsche Forschungsgemeinschaft through Sonderforschungsbereich SFB 1432 (Project No. 425217212, Subproject No. A07). The authors acknowledge DESY (Hamburg, Germany), a member of the Helmholtz Association HGF, for the provision of experimental facilities. Beamtime was allocated for proposal I-20231120. Funding for the HAXPES instrument at beamline P22 by the Federal Ministry of Education and Research (BMBF) under contracts 05KS7UM1 and 05K10UMA with Universität Mainz; 05KS7WW3, 05K10WW1, and 05K13WW1 with Universität Würzburg is gratefully acknowledged. Open access funding enabled and organized by Projekt DEAL.

### Data Availability Statement

The data that support the findings of this study are available from the corresponding author upon reasonable request.

### Conflicts of Interest

The authors declare no conflicts of interest.

1. T. S. Böscke, J. Müller, D. Bräuhäus, U. Schröder, and U. Böttger. 2011. "Ferroelectricity in hafnium oxide thin films," *Applied Physics Letters* 99, no. 10: 102903.
2. S. Fichtner, N. Wolff, F. Lofink, L. Kienle, and B. Wagner. 2019. "AlScN: A III-V semiconductor based ferroelectric," *Journal of Applied Physics* 125, no. 11: 114103.

3. T. Francois, et al. 2021. "16kbit HfO<sub>2</sub>:Si-based 1T-1C FeRAM Arrays Demonstrating High Performance Operation and Solder Reflow Compatibility," in *2021 IEEE International Electron Devices Meeting (IEDM)*, pp. 33.1.1–33.1.4.
4. H. Mulaosmanovic, E. T. Breyer, S. Dünkel, S. Beyer, T. Mikolajick, and S. Slesazek. 2021. "Ferroelectric field-effect transistors based on HfO<sub>2</sub>: a review," *Nanotechnology* 32, no. 50: 502002.
5. F. Ambriz-Vargas, et al. 2017. "A Complementary Metal Oxide Semiconductor Process-Compatible Ferroelectric Tunnel Junction," *ACS Applied Materials & Interfaces* 9, no. 15: 13262–13268.
6. A. Choupryk, D. Negrov, E. Y. Tsymlal, and A. Zenkevich. 2021. "Defects in ferroelectric HfO<sub>2</sub>," *Nanoscale* 13: 11635–11678.
7. Y. Zhou, et al. 2019. "The effects of oxygen vacancies on ferroelectric phase transition of HfO<sub>2</sub>-based thin film from first-principle," *Computational Materials Science* 167: 143–150.
8. C. Richter, et al. 2017. "Si Doped Hafnium Oxide—A "Fragile" Ferroelectric System," *Advanced Electronic Materials* 3, no. 10: 1700131.
9. S. Mueller, et al. 2012. "Incipient Ferroelectricity in Al-Doped HfO<sub>2</sub> Thin Films," *Advanced Functional Materials* 22, no. 11: 2412–2417.
10. G. Karbasian, et al. 2017. "Ferroelectricity in HfO<sub>2</sub> thin films as a function of Zr doping," in *2017 International Symposium on VLSI Technology, Systems and Application (VLSI-TSA)*, pp. 1–2.
11. R. Materlik, C. Künneth, M. Falkowski, T. Mikolajick, and A. Kersch. 2018. "Al-, Y-, and La-doping effects favoring intrinsic and field induced ferroelectricity in HfO<sub>2</sub>: A first principles study," *Journal of Applied Physics* 123, no. 16: 164101.
12. Y. Yun, et al. 2022. "Intrinsic ferroelectricity in Y-doped HfO<sub>2</sub> thin films," *Nature Materials* 21, no. 8: 903–909.
13. S. Mueller, C. Adelman, A. Singh, S. Van Elshocht, U. Schroeder, and T. Mikolajick. 2012. "Ferroelectricity in Gd-Doped HfO<sub>2</sub> Thin Films," *ECS Journal of Solid State Science and Technology* 1, no. 6: N123.
14. U. Schroeder, et al. 2018. "Lanthanum-Doped Hafnium Oxide: A Robust Ferroelectric Material," *Inorganic Chemistry* 57, no. 5: 2752–2765, PMID: 29446630.
15. T. Schenk, et al. 2013. "Strontium doped hafnium oxide thin films: Wide process window for ferroelectric memories," in *2013 Proceedings of the European Solid-State Device Research Conference (ESSDERC)*, pp. 260–263.
16. C.-Q. Luo, C.-Y. Kang, Y.-L. Song, W.-P. Wang, and W.-F. Zhang. 2021. "Large remanent polarization in Ta-doped HfO<sub>2</sub> thin films by reactive sputtering," *Applied Physics Letters* 119, no. 4: 042902.
17. Y. Maekawa, et al. 2024. "Ta<sup>5+</sup>-substitution effects on crystal structure and ferroelectric property in HfO<sub>2</sub>-based films," *Japanese Journal of Applied Physics*, 63, no. 9: 09SP17.
18. L. Baumgarten, et al. 2021. "Impact of vacancies and impurities on ferroelectricity in PVD- and ALD-grown HfO<sub>2</sub> films," *Applied Physics Letters* 118, no. 3: 032903.
19. T. Mittmann, et al. 2019. "Origin of Ferroelectric Phase in Undoped HfO<sub>2</sub> Films Deposited by Sputtering," *Advanced Materials Interfaces* 6, no. 11: 1900042.
20. A. Klein, et al. 2023. "The Fermi energy as common parameter to describe charge compensation mechanisms: A path to Fermi level engineering of oxide electroceramics," *Journal of Electroceramics* 51, no. 3: 147–177, Publisher Copyright: 2023, The Author(s).
21. M. H. Park, et al. 2017. "Effect of acceptor doping on phase transitions of HfO<sub>2</sub> thin films for energy-related applications," *Nano Energy* 36: 381–389.
22. C. Zhou, et al. 2024. "Enhanced polarization switching characteristics of HfO<sub>2</sub> ultrathin films via acceptor-donor co-doping," *Nature Communications* 15, no. 1: 2893.
23. L. Baumgarten, et al. 2023. "Smart Design of Fermi Level Pinning in HfO<sub>2</sub>-Based Ferroelectric Memories," *Advanced Functional Materials* 34: 3.
24. M. Müller, et al. 2022. "Hard x-ray photoelectron spectroscopy of tunable oxide interfaces," *Journal of Vacuum Science & Technology A* 40, no. 1: 013215.
25. T. Szyjka, et al. 2020. "Enhanced Ferroelectric Polarization in TiN/HfO<sub>2</sub>/TiN Capacitors by Interface Design," *ACS Applied Electronic Materials* 2, no. 10: 3152–3159.
26. O. Rehm, et al. 2024. "Long-Term Stability and Oxidation of Ferroelectric AlScN Devices: An Operando Hard X-ray Photoelectron Spectroscopy Study," *physica status solidi (RRL) – Rapid Research Letters*, 19, (3).
27. M. Trzhaskovskaya, and V. Yarzhemsky. 2018. "Dirac-Fock photoionization parameters for HAXPES applications," *Atomic Data and Nuclear Data Tables* 119: 99–174.
28. J. Robertson, and S. J. Clark. 2011. "Limits to doping in oxides," *Phys. Rev. B* 83: 075205.
29. T. Szyjka, et al. 2022. "From Doping to Dilution: Local Chemistry and Collective Interactions of La in HfO<sub>2</sub>," *physica status solidi (RRL) – Rapid Research Letters* 16: 10.
30. W. Hamouda, et al. 2020. "Physical chemistry of the TiN/Hf<sub>0.5</sub>Zr<sub>0.5</sub>O<sub>2</sub> interface," *Journal of Applied Physics* 127, no. 6: 064105.
31. W. Shockley, 1950. *Electrons and Holes in Semiconductors: With Applications to Transistor Electronics*. Bell Telephone Laboratories series, Van Nostrand.
32. C. Schlueter, et al. 2019. "The new dedicated HAXPES beamline P22 at PETRAIII," *AIP Conference Proceedings* 2054, no. 1: 040010.
33. W. S. M. Werner, W. Smekal, and C. J. Powell. 2017. *Simulation of electron spectra for surface analysis (SESSA) version 2.1 user's guide*. National Institute of Standards and Technology.